Redox Biology 52 (2022) 102303

Contents lists available at ScienceDirect

Redox Biology

journal homepage: www.elsevier.com/locate/redox

SSBP1 drives high fructose-induced glomerular podocyte ferroptosis via activating DNA-PK/p53 pathway

Wen-Yuan Wu [a], Zi-Xuan Wang [a], Tu-Shuai Li [a], Xiao-Qin Ding [a], Zhi-Hong Liu [a], Jie Yang [a], Lei Fang [b,**], Ling-Dong Kong [a,*]

[a] State Key Laboratory of Pharmaceutical Biotechnology, Institute of Chinese Medicine, Nanjing Drum Tower Hospital, School of Life Sciences, Nanjing University, Nanjing, PR China

[b] Jiangsu Key Laboratory of Molecular Medicine & Chemistry and Biomedicine Innovation Center, Medical School, Nanjing University, Nanjing, PR China

ARTICLE INFO

Keywords:
High fructose
Podocyte ferroptosis
SSBP1
DNA-PK
p53
Pterostilebene

ABSTRACT

High fructose consumption is a significant risking factor for glomerular podocyte injury. However, the causes of high fructose-induced glomerular podocyte injury are still unclear. In this study, we reported a novel mechanism by which high fructose induced ferroptosis, a newly form of programmed cell death, in glomerular podocyte injury. We performed quantitative proteomic analysis in glomeruli of high fructose-fed rats to identify key regulating proteins involved in glomerular injury, and found that mitochondrial single-strand DNA-binding protein 1 (SSBP1) was markedly upregulated. Depletion of SSBP1 could alleviate high fructose-induced ferroptotic cell death in podocytes. Subsequently, we found that SSBP1 positively regulated a transcription factor p53 by interacting with DNA-dependent protein kinase (DNA-PK) and p53 to drive ferroptosis in high fructose-induced podocyte injury. Mechanically, SSBP1 activated DNA-PK to induce p53 phosphorylation at serine 15 (S15) to promote the nuclear accumulation of p53, and thereby inhibited expression of ferroptosis regulator solute carrier family 7 member 11 (SLC7A11) in high fructose-exposed podocytes. Natural antioxidant pterostilebene was showed to downregulate SSBP1 and then inhibit DNA-PK/p53 pathway in its alleviation of high fructose-induced glomerular podocyte ferroptosis and injury. This study identified SSBP1 as a novel intervention target against high fructose-induced podocyte ferroptosis and suggested that the suppression of SSBP1 by pterostilbene may be a potential therapy for the treatment of podocyte ferroptosis in glomerular injury.

1. Introduction

The glomerular filtration barrier function is highly dependent on specific cells known as podocytes [1]. Loss of podocytes leads to albuminuria in many common glomerular diseases such as glomerulonephritis [2]. High fructose induces glomeruli lesions with podocyte injury and albuminuria [3,4]. However, the causes of high fructose-induced glomerular podocyte injury are still unclear.

Ferroptosis is a novel form of cell death driven by the iron-dependent peroxidation of lipids [5]. The morphological features of ferroptosis are obviously distinct from other types of programmed cell death. Mitochondrial membrane rupture is recognized as a typical characteristic of ferroptosis [6]. Solute carrier family 7 member 11 (SLC7A11) is active subunit of the cystine/glutamate antiporter system x_c^- [7]. Its low expression is reported to induce a decrease in cystine uptake and eventually cause a depletion of the major antioxidant glutathione (GSH) [8]. GSH is utilized by glutathione peroxidase 4 (GPX4) to convert lipid hydroperoxides to non-toxic lipid alcohols, and therefore protect cells from ferroptosis [9]. p53, a key tumor suppressor gene, functions as a transcription factor [10], participating in cellular events such as apoptosis, DNA repair, cell cycle regulation and senescence [11]. Recent study shows that SLC7A11 is a target of p53-mediated transcriptional repression [12]. $P53^{3KR}$, an acetylation-defective mutant, retains the ability to inhibit SCL7A11 expression and thereby induce ferroptotic cell death, but fails to cause cell-cycle arrest, senescence and apoptosis in erastin-stimulated lung cancer cells and mouse embryonic fibroblasts [12]. Ferroptosis inhibitor ferrostatin-1 can downregulate p53 expression and reduce cell death in podocyte-specific MDM2-knockout mice [13].

DNA-dependent protein kinase catalytic subunit (DNA-PKcs) and Ku70/Ku80 constitute DNA-PK, which is a major apical kinase in the

* Corresponding author. State Key Laboratory of Pharmaceutical Biotechnology, Nanjing University, Nanjing, 210023, PR China.
** Corresponding author. Medical School of Nanjing University, Nanjing University, Nanjing, 210093, PR China.
E-mail addresses: njfanglei@nju.edu.cn (L. Fang), kongld@nju.edu.cn (L.-D. Kong).

https://doi.org/10.1016/j.redox.2022.102303
Received 27 January 2022; Received in revised form 13 March 2022; Accepted 23 March 2022
Available online 31 March 2022
2213-2317/© 2022 Published by Elsevier B.V. This is an open access article under the CC BY-NC-ND license (http://creativecommons.org/licenses/by-nc-nd/4.0/).

Abbreviations

SSBP1	Single-strand DNA-binding protein 1
DNA-PK	DNA-dependent protein kinase
SLC7A11	Solute carrier family 7 member 11
GSH	Glutathione
GPX4	Glutathione peroxidase 4
DNA-PKcs	DNA-dependent protein kinase catalytic subunit
iTRAQ	Isobaric tags for relative and absolute quantification
mtDNA	Mitochondrial DNA
ROS	Reactive oxygen species
FBS	Fetal bovine serum
IFN-γ	Interferon γ
MDA	Malondialdehyde
NC	Negative control
LC-MS/MS	Liquid chromatography tandem mass spectrometry
Co-IP	Co-immunoprecipitation
mtROS	Mitochondrial ROS
MMP	Mitochondrial membrane potential

repair of DNA double-strand break and gene stability [14]. In high-fat diet-fed mice with nonalcoholic fatty liver disease, DNA-PKcs is activated to phosphorylate p53 at S15 and cause mitochondrial morphology disruption and dysfunction [15]. We and others have shown previously that high fructose increases p53 expression to induce liver fibrosis of rats and Jurkat cell apoptosis [16,17]. Nevertheless, whether DNA-PK/p53 pathway is involved in high fructose-induced podocyte ferroptosis in glomerular injury is poorly understood.

To discover key molecules that may be associated with high fructose-induced podocyte ferroptosis in glomerular injury, we thoroughly investigated the glomerular proteome profile of high fructose-fed rats [18]. Using isobaric tags for relative and absolute quantification (iTRAQ)-labeling technology followed by mass spectrometry analysis, we identified single-strand DNA-binding protein 1 (SSBP1) as a significantly upregulated protein. SSBP1 is required for stabilizing single-stranded DNA during mitochondrial DNA (mtDNA) replication [19]. mtDNA encodes the proteins related to the oxidative phosphorylation system, ribosomal RNAs and transfer RNAs. The reduction of mtDNA causes apoptosis or pyroptosis in angiotensin II-exposed bone marrow mescenchymal stem cells or hypoxia-stimulated cardiomyocytes [20,21]. Moreover, SSBP1 mutation is observed in kidney insufficiency and chronic kidney disease in patients, with mtDNA deletion and subsequently mitochondrial dysfunction [22,23]. Recently, SSBP1 overexpression is reported to reduce cell viability in angiotensin II-induced fibroblasts [24]. However, the functional role of SSBP1 on DNA-PK/p53 pathway in high fructose-induced glomerular podocyte ferroptosis remains unclear.

In this study, we demonstrated that SSBP1 is an accelerant of high fructose-induced ferroptosis in glomerular injury. Furthermore, we identified p53 as a novel SSBP1 effector, likely through enhancing p53 phosphorylation by DNA-PK and its nuclear accumulation to repress SLC7A11 expression, subsequently drive podocyte ferroptosis. The accumulation of lipid reactive oxygen species (ROS) can induce cell ferroptosis [5]. Pterostilbene, a natural antioxidant, is reported to inhibit ROS-mediated mitochondrial apoptosis in hepatocellular carcinoma [25]. Our previous study showed that pterostilbene attenuated high fructose-induced rat renal oxidative stress and fibrosis [26,27]. Interestingly, pterostilbene was found to downregulate SSBP1 and suppress DNA-PK/p53 pathway in the alleviation of high fructose-induced podocyte ferroptosis. Therefore, the suppression of SSBP1 may be a potential therapy for the treatment of podocyte ferroptosis in glomerular injury.

2. Methods and materials

2.1. Reagents and antibodies

Pterostilbene (≥99%), pioglitazone (≥99%), and hoechst were purchased from Sigma-Aldrich (Saint Louis, USA). Urine protein test and creatinine assay kits were purchased from Jiancheng (Nanjing, China). Apoptosis detection, periodic acid-schiff staining, GSH and GSSG assay, mitochondrial membrane potential assay, and nuclear and cytoplasmic protein extraction kits were purchased from Beyotime (Shanghai, China). Fetal bovine serum (FBS) was purchased from Wisent (Saint Bruno, Canada). Penicillin/streptomycin and MitoTracker® Deep Red FM were purchased from Invitrogen (Carlsbad, USA). Recombinant interferon γ (IFN-γ) was purchased from R&D Systems (Minneapolis, USA). Propidium iodide was purchased from Fcmacs Biotechnology (Nanjing, China). Ferroptosis inhibitor ferrostatin-1 was purchased from Ark Pharm (Chicago, USA). Iron chelator deferoxamine was purchased from TargetMol (Shanghai, China). C11-BODIPY (581/591), TRIzol reagent, Lipofectamine 2000 regent, RPMI culture medium, classic magnetic IP/Co-IP kit, BCA protein assay kit, Alexa Fluor 555 goat *anti*-rabbit and Alexa Fluor 488 goat *anti*-mouse secondary antibody were purchased from Thermo Fisher Scientific (Waltham, USA). Malondialdehyde (MDA) assay kit was purchased from Solarbio (Beijing, China). HiScript® II Q RT SuperMix, ChamQ™ SYBR® qPCR Master Mix and cell/tissue DNA isolation kit were purchased from Vazyme (Nanjing, China). PCR primers, siRNA and respective negative control (NC) were synthesized from GenePharma (Shanghai, China). Plasmids and respective NC were synthesized from Abiocenter (Beijing, China). MitoSOX red mitochondrial superoxide indicator was purchased from Yeasen (Shanghai, China). DNA-PK kinase enzyme system and ADP-Glo kinase assay kits were purchased from Promega (Wisconsin, USA). DNA-PK inhibitor LTURM34 was purchased from Glpbio (Montclair, USA). *Anti*-synaptopodin (MAB4919) was purchased from Abnova Corporation (Taipei, Taiwan). *Anti*-IgG (ab172730), *anti*-SSBP1 (ab224053), *anti*-p53 (ab1101), *anti*-p-p53(S15) (ab223868), *anti*-DNA-PKcs (ab44815), *anti*-p-DNA-PKcs(S2056) (ab124918) and *anti*-Lamin B1(ab16048) were purchased from Abcam (Cambridge, USA). Anti-p53 (60283-2-Ig), *anti*-GPX4 (66763-1-Ig), *anti*-SLC7A11 (26864-1-AP), *anti*-Myc Tag (16286-1-AP), anti-Flag Tag (80010-1-RR), anti-HA Tag (51064-2-AP), *anti*-GAPDH (10494-1-AP), HRP-conjugated anti-mouse (SA00001-1) and anti-rabbit secondary antibody (SA00001-2) were purchased from Proteintech (Chicago, USA). Anti-SSBP1 (GTX55806) was purchased from GeneTex (San Antonio, USA). Enhanced chemiluminescence detection kit was purchased from Tanon (Shanghai, China).

2.2. Animal model

In this study, all animal experiments were approved by the Institutional Animal Care and Use Committee of Nanjing University. Five-week-old male Sprague-Dawley rats (180–220 g) were provided from the Beijing Weitong Lihua Laboratory Animal Technology Co., Ltd (Beijing, China). Rats were housed in the environment with relative humidity of 50 ± 5%, at the constant temperature (22 ± 2) °C with a normal 12-h light/dark cycle and had access to the food and water freely before experiment. Rats were assigned into control group with a standard water, and high fructose group fed with 10% fructose solution (W/V) for 4, 8, 12 and 16 weeks, respectively. At indicated time intervals (4, 8, 12 and 16 weeks), rats randomly selected from control group and high fructose group respectively, were used for subsequent experiments. For drug intervention, rats were assigned into control group with a standard water and high fructose group treated with 10% fructose solution (W/V) for 16 weeks. After 8-week fructose intake, high fructose group rats were randomized into 5 subgroups, receiving water (vehicle), 10, 20 and 40 mg/kg pterostilbene, and 4 mg/kg pioglitazone via daily intragastric gavage (10 mL/kg) for the next 8 weeks. At 11th week, urine of rats was collected in metabolism cages, centrifuged at 3000×*g* for 10 min and

stored at -80 °C. After rats were anesthetized, rat kidney cortex tissues were cut into pieces for the following experiments and stored at -80 °C. Isolation of rat glomeruli was isolated by the graded sieving technique as we reported previously [18].

2.3. Cell culture and treatment

Conditionally immortalized human podocytes were gifted from Dr. Zhi-Hong Liu (Research Institute of Nephrology, Nanjing General Hospital of Nanjing Military Command, Nanjing, China). Human glomerular mesangial and endothelial cells were obtained from Cell Bank of Chinese Academy of Sciences (Shanghai, China). Human podocytes were cultured under permissive conditions (at 33 °C) in RPMI culture medium containing 10% FBS and 1% penicillin/streptomycin and 10 U/ml recombinant IFN-γ. Human podocytes were then differentiated at 37 °C in RPMI medium with 10% FBS and 1% penicillin/streptomycin for 7 days. Human glomerular mesangial and endothelial cells were cultured in DMEM medium with 10% FBS and 1% penicillin/streptomycin at 37 °C. After treated with fructose (5 mM) for 0, 24, 48, 72 or 96 h, cells were analyzed in various experiments as described below. For drug intervention, cells were treated with or without fructose (5 mM), pterostilbene (10 μM) or pioglitazone (10 μM) for 96 h, respectively.

2.4. Cell death assay

kidneys were fixed with 4% paraformaldehyde, embedded in paraffin and then cut at 4 μm thick for TUNEL staining. For the detection of TUNEL-positive cells, the *in situ* apoptosis detection kit was used according to the manufacturer's instructions. The glomeruli were stained with synaptopodin antibody and Alexa Fluor 488 goat *anti*-mouse secondary antibody (red). The nuclei were stained with hoechst (blue). The green fluorescence of dead cells in rat glomeruli was detected with confocal laser scanning microscope (LSM-880, Carl Zeiss, Oberkochen, Germany).

The differentiated podocytes were collected, centrifuged at 500×*g* for 5 min and washed twice with PBS. The washed podocytes were suspended in PBS and stained with propidium iodide staining (20 μg/mL) in the dark at 37 °C for 20 min. Podocytes were then washed with PBS and analyzed by cytometer analysis. Cell death was calculated the percentage of podocytes with propidium iodide fluorescence.

2.5. Histology

kidneys were fixed with 4% paraformaldehyde, embedded in paraffin and then cut at 4 μm thick for periodic acid-schiff (PAS) staining. PAS staining was done using with periodic acid-schiff staining kit according to the manufacturer's instructions. Mesangial expansion was scored based on percent of glomeruli with mesangial expansion (%), performed in a double-blinded manner [28].

2.6. Biochemical analysis

As described previously [3], the level of urinary albumin was detected using urine protein test kit, and the level of urinary creatinine was detected using creatinine assay kit according to the manufacturer's instructions, respectively. The level of urinary albumin was corrected according urinary creatinine value.

The level GSH and GSSG was detected using GSH and GSSG assay kit according to the manufacturer's instructions, respectively. Briefly, differentiated podocytes were collected, lysed and centrifuged at 10,000×*g* for 10 min. Then, we firstly divided one sample into two equal aliquots, one for measuring total (GSH + GSSG) level and the other for measuring only GSSG level after removing GSH. Each aliquot was mixed with GSH assay buffer, 5,5′-dithio-bis 2-nitrobenzoic acid solution, GSH reductase and incubated at 25 °C for 5 min, followed by adding NADPH, respectively. The absorbance was measured at a wavelength of 410 nm on a microplate reader. Subsequently, the concentration of GSH was calculated as: GSH = total (GSH + GSSG) - GSSG. The GSH level was quantified relative to protein concentration.

MDA level was detected using MDA assay kit according to the manufacturer's instructions. The supernatant of podocyte lysates and the MDA detection agent were heated in water both at 100 °C for 15 min. Then, the mixture was centrifuged at 1000×*g* for 10 min. The absorbance was measured at a wavelength of 450, 532 and 600 nm on a microplate reader. The MDA level was calculated as: MDA = 5 × (12.9 × (A_{532} - A_{600}) - 2.58 × A_{450}). The MDA level was quantified relative to protein concentration.

Differentiated podocytes were collected and rinsed with PBS. Then, podocytes were incubated with C11-BODIPY staining (2.5 μM) solution in the dark at 37 °C for 30 min. Podocytes were rinsed with PBS and analyzed by Attune NxT flow cytometer analysis (Invitrogen). Lipid peroxidation was calculated as C11-BODIPY fluorescence intensity.

2.7. Mitochondrial morphology and function

Genomic DNA of rat glomeruli and differentiated podocytes were extracted by using cell/tissue DNA isolation kit, respectively. mtDNA copy number was measured using the quantitative real-time PCR. The primers used in this study were as follows: h-*mtDNA* F: CCCTAACACCAGCCTAACCA; h-*mtDNA* R: AAAGTGCATACCGCCAAAAG; h-*HBB* F: CTATGGGACGCTTGATGT; h-*HBB* R: GCAATCATTCGTCTGTTT; r-*mtDNA* F: ACACCAAGGTTAATGTAGC; r-*mtDNA* R: TTGAATCCATCTAAGCATT; r-*HBB* F: CAGTACTTTAAGTTGGAAACG; r-*HBB* R: ATCAACATAATTGCAGAGC. mtDNA content was quantified relative to the nuclear *HBB* gene [29].

Transmission Electron Microscope was used to observe mitochondrial morphology of glomerular podocytes. Differentiated podocytes were stained by MitoTracker® Deep Red FM to detect the changes of mitochondrial morphology. Mitochondria were divided into three categories to quantify morphological changes as described in the report [30]. Healthy podocytes having long tubules mitochondria were assigned to category I. Podocytes containing large round dotted mitochondria distributed throughout the cytosol were defined as category II. Podocytes with totally fragmented mitochondria close to the nucleus represented category III. Images were acquired using confocal laser scanning microscope (LSM-880, Carl Zeiss, Oberkochen, Germany).

Mitochondrial ROS (mtROS) was detected by MitoSOX red mitochondrial superoxide indicator according to the instructions of the manufacturer. Differentiated podocytes were collected, centrifuged at 500×*g* for 5 min and washed twice with PBS. Next, podocytes were loaded with MitoSOX reagent (5 μmol/L) in the dark at 37 °C for 30 min. Podocytes were then washed gently three times with PBS and analyzed by cytometer analysis. mtROS level was calculated as MitoSOX fluorescence intensity.

Mitochondrial membrane potential (MMP) was measured by mitochondrial membrane potential assay kit according to the instructions of the manufacturer. Differentiated podocytes were collected, centrifuged at 500×*g* for 5 min and washed twice with PBS. Next, podocytes were incubated with JC-1 dye (10 μg/mL) in the dark at 37 °C for 20 min. Podocytes were then washed gently three times with PBS and analyzed by cytometer analysis with aggregates (indicative of normal membrane potential) and the monomers (indicative of loss of membrane potential). MMP was analyzed by the ratio of aggregates/monomers intensity.

2.8. DNA-PK activity assay

The activity of DNA-PK was determined using the DNA-PK kinase enzyme system and ADP-Glo kinase assay kit according to the manufacturer's protocols. Briefly, differentiated podocyte lysates with the kinase reaction were incubated at room temperature for 60 min. The amount of ADP production was detected using ADP-Glo kinase assay, and the luminescence intensity was then measured using a microplate

luminometer.

2.9. Liquid chromatography tandem mass spectrometry (LC-MS/MS)

Glomerular proteins of high fructose-fed rats were extracted. The protein concentration was measured and further confirmed by Coomassie brilliant blue staining. After trypsin digestion, the peptides were labeled with iTRAQ Reagent 8-plex multiplex kit (SCIEX) for LC-MS/MS analysis and the data was deposited to the ProteomeXchange Consortium (http://www.proteomexchange.org) with the dataset identifier PXD017849 as previously described [18].

The proteins were evaluated by SDS-PAGE and visualized by Coomassie brilliant blue staining. The gel bands of interest were cut and in-gel digested by adding trypsin at 37 °C overnight. The digested peptides were then extracted from gel pieces and subjected to liquid chromatography tandem-mass spectrometry. LC-MS/MS was carried out by nanoflow liquid chromatography (Eksigent, CA) coupled on-line to a TripleTOF 5600^{+} mass spectrometer (SCIEX).

2.10. Western blot analysis

Nuclear and cytoplamic protein extracts from rat glomeruli or differentiated podocytes using nuclear and cytoplasmic protein extraction kit according to the manufacturer's instructions. Total proteins of rat glomeruli or differentiated podocytes were extracted in RIPA lysis buffer with PSMF (0.1 mM) and then centrifuged at 10,000×*g* for 10 min. The protein concentration was determined by BCA protein assay kit according to the manufacturer's instructions.

Western blot analysis was performed essentially as described previously [3]. An equal amount of protein (20 μg) was electrophoresed in 8–12.5% SDS-PAGE and then transferred to the PVDF membrane. The membranes were blocked with 5% milk for 2 h and incubated with primary antibodies overnight at room temperature. Antibodies specific for *anti*-GPX4, *anti*-SLC7A11, *anti*-SSBP1, *anti*-p53, *anti*-p-p53(S15), *anti*-DNA-PKcs *anti*-p-DNA-PKcs(S2056), *anti*-Myc Tag, *anti*-Flag Tag, *anti*-HA Tag, *anti*-Lamin B1 and *anti*-GAPDH. After washing, the membranes were incubated with HRP-conjugated *anti*-mouse and *anti*-rabbit secondary antibody for 1 h. The blots were visualized via enhanced chemiluminescence dectection kit and quantified via densitometry using ImageJ (version 1.42q, National Institutes of Health).

2.11. Quantitative real-time PCR

Total RNA was isolated from the rat glomeruli and differentiated podocytes with TRIzol. First-strand cDNA was synthesized using HiScript® II Q RT SuperMix. qRT-PCR was performed with ChamQ™ SYBR® qPCR Master Mix in a CFX Connect Real-Time PCR Detection System (Bio-Rad). The primers used in this study were as follows: h-*SSBP1* F: AAAAGACAACATGGCACAGA; h-*SSBP1* R: TCCAAATAAATTCGAGACCC; h-*p53* F: GCGTGTTTGTGCCTGTCCTG; h-*p53* R: GTGCTCGCTTAGTGCTCCCT; h-*β-actin* F: CATGTACGTTGCTATCCAGGC; h-*β-actin* R: CTCCTTAATGTCACGCACGAT; r-*SSBP1* F: GCCAGCAGTTTGGTTCTT; r-*SSBP1* R: TTTCCCTCCACCTGTCTC; r-*p53* F: GCGTTGCTCTGATGGTGA; r-*p53* R: CAGCGTGATGATGGTAAGGA; r-*β-actin* F: GAGAGGGAAATCGTGCGT; r-*β-actin* R: GGAGGAAGAGGATGCGG. The mRNAs were normalized to *β-actin*.

2.12. siRNA and plasmid transfection

SSBP1 siRNA F: GGCAUAUCAAUAUGUGAAATT; *SSBP1* siRNA R: UUUCACAUAUUGAUAUGCCTT; DNA-PKcs siRNA F: UUGACAUACUCCUCCUGCGTT; DNA-PKcs siRNA R: CUUUAUGGUGGCCAUGGAGTT; NC F: UUCUCCGAACGUGUCACGUTT; NC R: ACGUGACACGUUCGGAGAATT. The cDNA for the following full-length proteins with an epitope tag at the C-terminal were commercially synthesized: Flag-tagged full-length *SSBP1*, Myc-tagged full length *p53* (Myc-Wt *p53*) and HA-tagged full-length *DNA-PKcs*. These genes were cloned into the pcDNA3.1 vector. Myc-tagged mutant *p53* (Myc-Mut *p53*) was obtained by mutating Ser to Ala at amino acid 15 of p53. For *SSBP1* plasmid, full length *SSBP1* was subcloned into pcDNA3.1 vector. NC of plasmid was pcDNA3.1 vector. Lipofectamine 2000 was used for siRNA or plasmid transfection according to the manufacturer's protocols.

2.13. Co-immunoprecipitation (Co-IP)

Co-IP assay was carried out using classic magnetic IP/Co-IP kit according to the instructions of the manufacturer. Podocyte lysates in IP lysis buffer were incubated with Co-IP antibody against SSBP1 or HA Tag rotationally at 4 °C overnight. IgG was as control. The immune complex solution was incubated with protein A/G magnetic beads with shaking for 1 h at room temperature and then washed with elution buffer to remove unbound immune complex. The binding proteins were dissociated from the beads with low-pH buffer for LC-MS/MS or Western blot analysis.

2.14. Immunofluorescence assay

Differentiated podocytes were fixed with 4% paraformaldehyde and blocked with 10% FBS and 0.2% Triton X-100. Cells were stained with the primary SSBP1 or p53 antibody overnight at room temperature, then with Alexa Fluor 555 goat *anti*-rabbit or Alexa Fluor 488 goat *anti*-mouse secondary antibody for 1 h, and with hoechst for 10 min. Immunofluorescence images were captured by a confocal microscope.

2.15. Statistical analysis

Data were presented as mean ± SEM from at least 3 repeated experiments (n = 3) unless otherwise described. Statistical significance (*P* values) was calculated by two-tailed unpaired Student *t*-test, or One-Way ANOVA with Dunnett's post hoc test using Graphpad Prism 8. Difference was considered significant at $P < 0.05$.

3. Results

3.1. High fructose induces podocyte ferroptosis in glomerular injury

As reported by us and others previously, high fructose induces glomerular injury with proteinuria and mesangial expansion [3,31–33]. Here, we established a rat model fed with high fructose for 4, 8, 12 and 16 weeks, and also observed that high fructose increased the ratio of urinary albumin to creatinine in rats at 12th and 16th week (Supplemental Fig. 1A). PAS staining of kidney cortex sections revealed an increased mesangial expansion in high fructose-dieted rats at 12th and 16th week (Supplemental Fig. 1B-C). These data further demonstrated that high fructose induced progressive glomerular injury.

Next, we observed cell death in high fructose-stimulated rat glomeruli and cultured podocytes (Fig. 1A-B). Ferroptosis inhibitor ferrostatin-1 and iron chelator deferoxamine could attenuate high fructose-induced cell death in cultured podocytes (Fig. 1C). The fluorescence intensity of C11-BODIPY for the determination of lipid peroxidation was increased in high fructose-cultured podocytes (Fig. 1D). Similarly, MDA, the end product of lipid peroxidation, was increased in high fructose-stimulated rat glomeruli and cultured podocytes (Fig. 1E-F), with GSH reduction (Supplemental Fig. 1D-E). Meanwhile, SLC7A11 and GPX4, protein markers of ferroptosis, were downregulated in *in vivo* and *in vitro* models (Fig. 1G-H and Supplemental Fig. 1F-G). These data indicated that ferroptosis was activated in high fructose-induced glomerular podocyte injury.

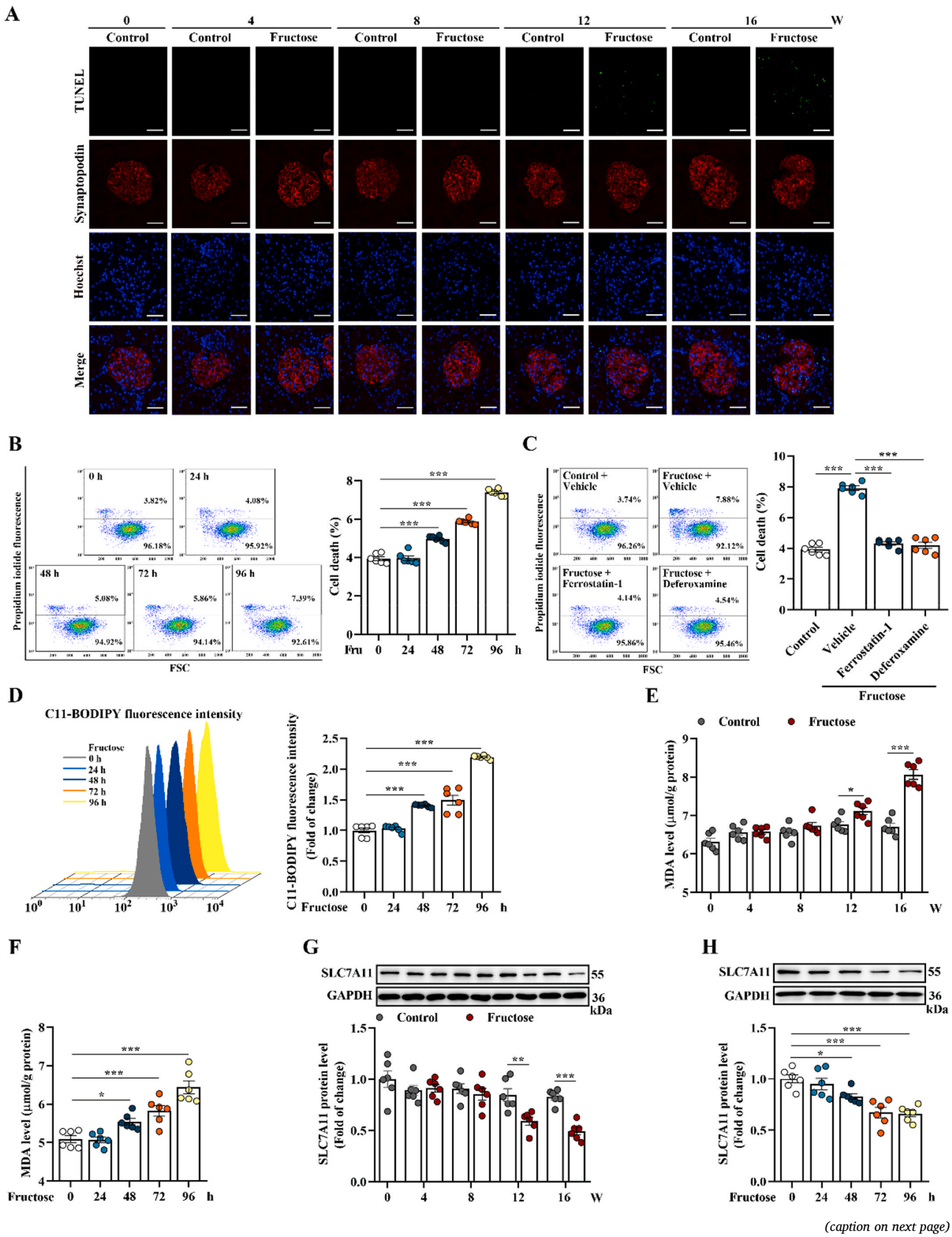

(caption on next page)

Fig. 1. High fructose induces podocyte ferroptosis in glomerular injury. (A) Rats were fed with water (control group) or 10% fructose solution (W/V) (high fructose group) for 4, 8, 12 and 16 weeks, respectively. Cell death in rat glomeruli was analyzed by TUNEL staining. Green fluorescence in pictures represented positive signals (cell death) (scale bars: 20 μm) (n = 3 per group). (B) Podocytes were cultured with fructose (5 mM) for 0, 24, 48, 72 or 96 h. Podocyte death was analyzed by propidium iodide staining and measured by flow cytometer (n = 6 per group). (C) Podocytes were cultured with or without fructose (5 mM) and in the presence or absence of ferroptosis inhibitors ferrostatin-1 or deferoxamine. Podocyte death was analyzed by propidium iodide staining and measured by flow cytometer (n = 6 per group). (D) Lipid peroxidation in high fructose-cultured podocytes was analyzed by C11-BODIPY (581/591) staining and measured by flow cytometer (n = 6 per group). (E–F) The MDA level was measured by assay kit in high fructose-exposed rat glomeruli and podocytes (n = 6 per group). (G–H) Western blot analysis of the protein level of SLC7A11 in rat glomeruli and podocytes (n = 6 per group). Data are plotted as mean ± SEM. *P*-values were acquired by one-way ANOVA, $^{*}P < 0.05$, $^{**}P < 0.01$, $^{***}P < 0.001$.

3.2. SSBP1 triggers podocyte ferroptosis in high fructose-induced glomerular injury

As we reported previously [18], to identify key proteins involved in high fructose-induced glomerular injury, we analyzed glomeruli from the rat model using an iTRAQ-based quantitative proteomic approach. Since significant changes of high fructose-induced glomerular injury and podocyte ferroptosis appeared at 12th and 16th week, we mainly investigated these two time-points of animal model. Among hundreds of dysregulated proteins in high fructose-dieted group compared with

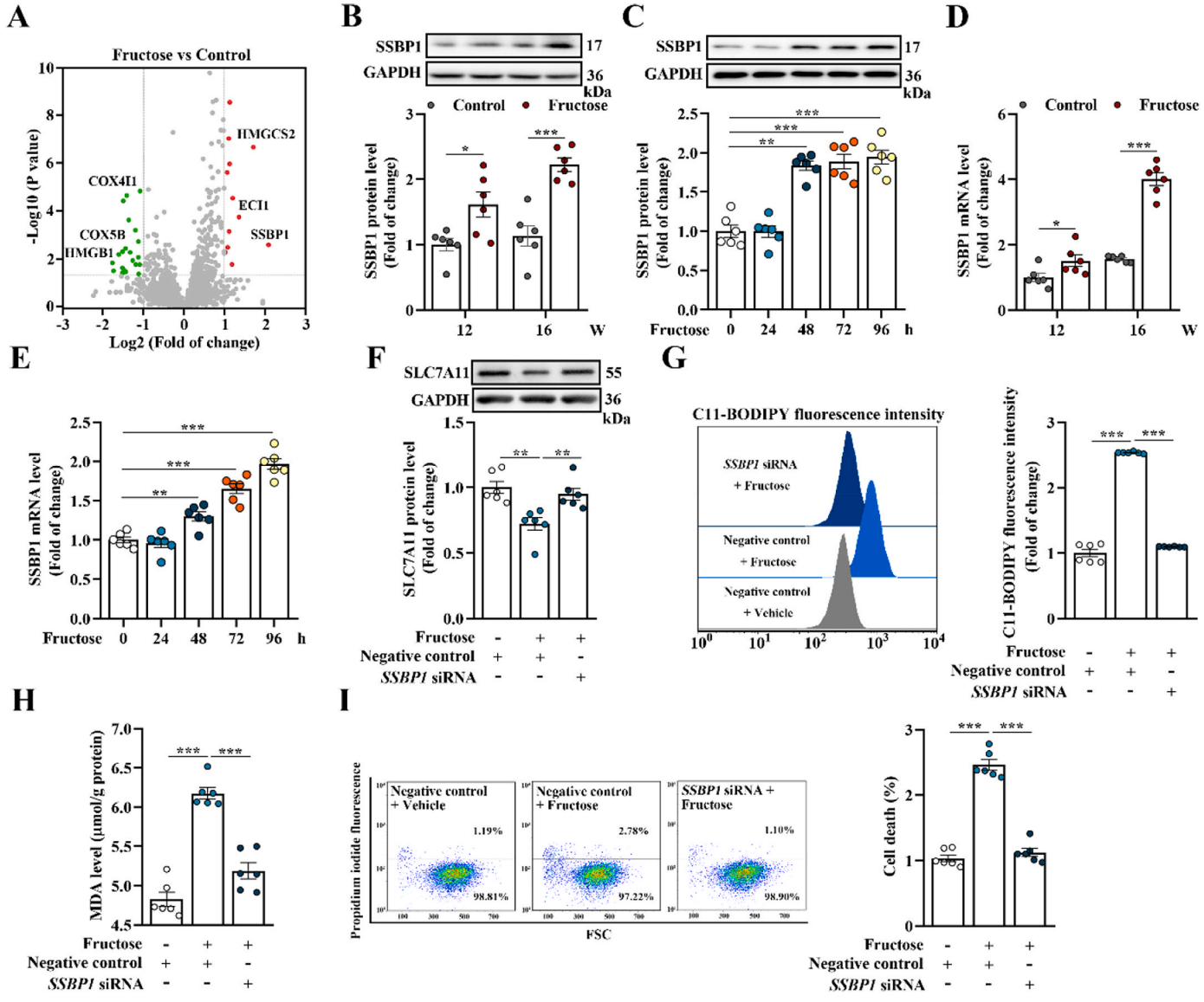

Fig. 2. SSBP1 triggers podocyte ferroptosis in high fructose-induced glomerular injury. (A) Dysregulated proteins in high fructose-stimulated rat glomeruli at 16th week were identified by iTRAQ-based quantitative proteomic analysis. Differences were considered statistically significant when fold change >2 (red) or < 0.5 (green) and $P < 0.05$. (B–C) Western blot analysis of the protein level of SSBP1 in high fructose-stimulated rat glomeruli and podocytes (n = 6 per group). (D–E) The mRNA level of SSBP1 was measured by qPCR in high fructose-exposed rat glomeruli and podocytes (n = 6 per group). (F–I) Podocytes were transfected with *SSBP1* siRNA as well as negative control and then cultured with vehicle or fructose (5 mM). Western blot analysis of the protein level of SLC7A11 in podocytes (n = 6 per group). Lipid peroxidation in podocytes was analyzed by C11-BODIPY (581/591) staining and measured by flow cytometer (n = 6 per group). The MDA level was measured by assay kit in podocytes (n = 6 per group). Podocyte death was analyzed by propidium iodide staining and measured by flow cytometer (n = 6 per group). Data are plotted as mean ± SEM. *P*-values were acquired by one-way ANOVA, $^{*}P < 0.05$, $^{**}P < 0.01$, $^{***}P < 0.001$.

control group, we focused on one interesting candidate protein, SSBP1, which was remarkably upregulated in glomeruli of fructose-dieted rat at 16th week (Fig. 2A and Supplemental Table 1). Western blot analysis further confirmed the upregulation of SSBP1 in glomeruli of rat model at 12th and 16th week (Fig. 2B). Of note, although its protein expression was generally observed in the three major cell types of glomeruli including podocytes, mesangial and endothelial cells, SSBP1 was specifically upregulated only in high fructose-cultured podocytes (Fig. 2C and Supplemental Fig. 2A-B). In accordance with iTRAQ and Western blot results, significant upregulation of SSBP1 mRNA level was also observed in high fructose-stimulated rat glomeruli and cultured podocytes (Fig. 2D-E). However, there was no obvious changes of SSBP1 mRNA level in high fructose-induced mesangial and endothelial cells (Supplemental Fig. 2C-D).

As SSBP1 is essential for mtDNA replication [34], we assessed the mtDNA content by specific primers. We found that the mtDNA copy number in high fructose-exposed rat glomeruli and cultured podocytes was significantly decreased, compared with control group (Supplemental Fig. 2E-F). It is reported that SSBP1 mutation causes mitochondrial morphology disruption and dysfunction in retinas and primary fibroblasts of patients with optic atrophy, which are characteristics of ferroptosis [22,35]. Therefore, we observed whether mitochondrial morphology and function were affected in this study. In line with our previous study [18], ultrastructure of mitochondria revealed mitochondrial membrane rupture and disappearance of cristae in high fructose-dieted rat glomerular podocytes at 16th week (Supplemental Fig. 2G). Furthermore, we observed changes of mitochondrial morphology from long tubules to fragmentation in high fructose-cultured podocytes (Supplemental Fig. 2H). According to classification system of mitochondrial morphology from other study [30], the quantification of mitochondrial shape showed a significant increase in cultured podocytes of category III after 48 h fructose exposure (Supplemental Fig. 2I). For mitochondrial function, we examined the level of mtROS and MMP, and observed remarkable increase of mtROS and loss of MMP in high fructose-cultured podocytes (Supplemental Fig. 2J-K).

To further investigate the role of SSBP1 in high fructose-induced glomerular podocyte ferroptosis, cultured podocytes were transfected with *SSBP1* siRNA and then incubated with high fructose. We found that SSBP1 knockdown in high fructose-cultured podocytes significantly increased protein expression of SLC7A11 and GPX4 (Fig. 2F and Supplemental Fig. 2L-N). Depletion of SSBP1 increased GSH, and decreased lipid peroxidation and MDA in high fructose-cultured podocytes (Fig. 2G-H and Supplemental Fig. 2O). SSBP1 knockdown also decreased ferroptotic cell death in this cell model (Fig. 2I). Therefore, SSBP1 may trigger podocyte ferroptosis in high fructose-caused glomerular injury.

3.3. SSBP1 interacts with p53 and facilitates p53 S15 phosphorylation to increase accumulation of nuclear p53 in high fructose-stimulated glomerular podocyte ferroptosis

To explore the possible molecular mechanism by which SSBP1 induced ferroptosis, we investigated SSBP1 associating proteins in high fructose-cultured podocytes using Co-IP coupled with mass spectrometry analysis. Notably, we identified p53 and DNA-PKcs in the SSBP1 protein complex Co-IP from high fructose-cultured podocytes (Supplemental Table 2 and Supplemental Fig. 3A). As an upstream transcription factor regulating SLC7A11 [11], p53 interaction with SSBP1 was further confirmed in high fructose-cultured podocytes using the antibody specifically against p53 after Co-IP (Fig. 3A).

Next, we investigated whether SSBP1 modulated p53 expression in podocytes. Overexpression or knockdown of SSBP1 showed no significant effect on p53 mRNA level in cultured podocytes (Fig. 3B-C and Supplemental Fig. 3B-C). SSBP1 overexpression remarkably enhanced total p53 protein expression, while inverse effects were observed in SSBP1-depleted podocytes (Fig. 3D-E). We also observed upregulation of total p53 in high fructose-exposed rat glomeruli and cultured podocytes (Fig. 3F-G). However, p53 mRNA had no obvious change in *in vivo* and *in vitro* models (Supplemental Fig. 3D-E). p53 is reported to occupy the promoter region of the SLC7A11 gene to mediate transcriptional repression [12]. Thus, we evaluated whether p53 was accumulated in cell nucleus. Western blot analysis showed relatively high levels of nuclear p53 in high fructose-stimulated rat glomeruli and cultured podocytes (Fig. 3H-I). The immunofluorescence staining showed nuclear accumulation of p53 stimulated by high fructose and also revealed the co-localization of SSBP1 and p53 proteins in high fructose-exposed podocytes (Fig. 3J). Since post-translational modification of p53 can regulate its nuclear import/export [36], we then examined the p53 phosphorylation. We observed that p53 S15 phosphorylation was notably increased in high fructose-exposed rat glomeruli and cultured podocytes (Fig. 3K-L). Nuclear/cytoplasmic separation assay of cultured podocytes transfected with Myc-Wt p53 or Myc-Mut p53 indicated that p53 S15 phosphorylation was crucial for its nuclear translocation with or without high fructose stimulation (Fig. 3M). Thus, we determined whether SSBP1 facilitated p53 phosphorylation and nuclear accumulation after high fructose exposure. We found that knockdown of SSBP1 decreased p53 S15 phosphorylation level and inhibited p53 nuclear accumulation in high fructose-cultured podocytes (Fig. 3N-P). These data indicated that SSBP1 may promote p53 translocation into the nuclei by facilitating p53 S15 phosphorylation in high fructose-stimulated glomerular podocyte ferroptosis.

3.4. SSBP1 activates DNA-PK to phosphorylate p53 in high fructose-induced glomerular podocytes ferroptosis

p53 can be phosphorylated by different cellular kinases [37,38], so we wondered which kinase phosphorylated p53 at S15 in high fructose-exposed glomerular podocytes. Mass spectrometry analysis of proteins Co-IP with SSBP1 revealed an interaction between SSBP1 and DNA-PKcs (Supplemental Table 2 and Supplemental Fig. 3A). It is reported that DNA-PKcs, the catalytic subunit of DNA-PK, mediates S15-phosphorylation of p53 [39]. In this study, DNA-PKcs interaction with SSBP1 was further confirmed in high fructose-cultured podocytes using the antibody specifically against DNA-PKcs after Co-IP (Fig. 4A). The overexpression of SSBP1 in cultured podocytes obviously increased DNA-PK activity and DNA-PKcs phosphorylation (Fig. 4B-C). SSBP1 knockdown could decrease DNA-PK activity and DNA-PKcs phosphorylation in cultured podocytes (Fig. 4D-E). Subsequently, we observed that DNA-PK activity and DNA-PKcs phosphorylation were upregulated simultaneously in high fructose-exposed rat glomeruli and cultured podocytes (Fig. 4F-H), which were reversed by inhibition of SSBP1 with siRNA (Fig. 4I-J). Of note, we transiently expressed Flag-SSBP1, Myc-p53 and HA-DNA-PKcs alone or in combination in cultured podocytes and performed Co-IP assay, and found that DNA-PKcs robustly co-eluted with SSBP1 and p53 (Fig. 4K). Furthermore, we investigated the interaction of SSBP1 and p53 in high fructose-cultured podocytes in the absence of DNA-PKcs, and found that DNA-PKcs knockdown reduced SSBP1 and p53 interaction in high fructose-cultured podocytes (Supplemental Fig. 4A-C).

Thus, we focused on the role of DNA-PK in p53-regulated ferroptosis in high fructose-induced podocyte injury. Upregulation of fructose-induced p53 phosphorylation and nuclear p53 protein level were attenuated by DNA-PK inhibitor LTURM34 (Fig. 4L-M). Consistently, inhibition of DNA-PK by LTURM34 upregulated SLC7A11 and GPX4 protein levels (Fig. 4N and Supplemental Fig. 4D), as well as increased GSH, and decreased lipid peroxidation and MDA (Fig. 4O-P and Supplemental Fig. 4E) in high fructose-cultured podocytes. Subsequently, DNA-PK inhibition decreased ferroptotic cell death in high fructose-exposed podocytes (Fig. 4Q). Thus, DNA-PK may participate in SSBP1-drived ferroptosis through phosphorylating p53 in high fructose-induced glomerular podocyte injury.

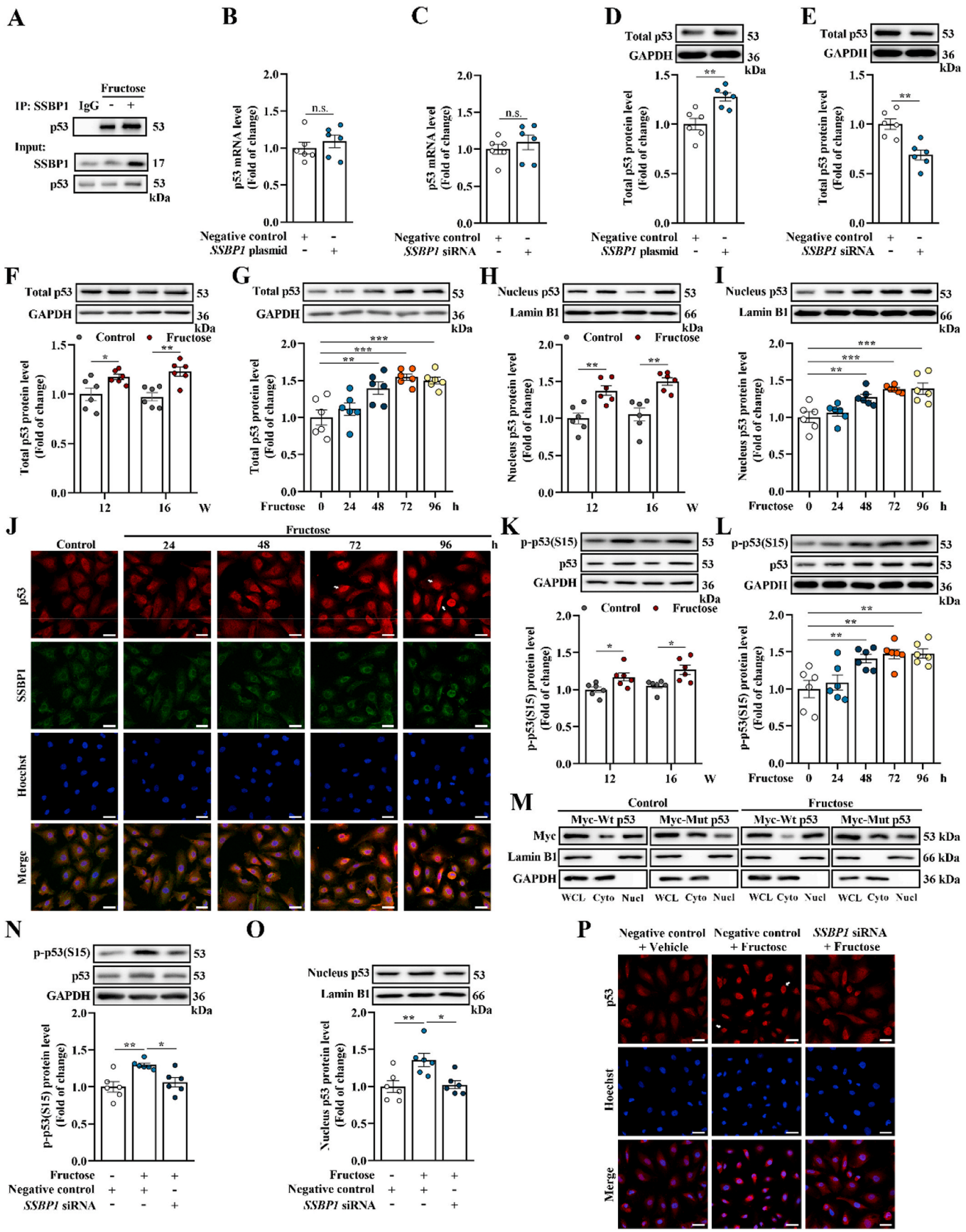

(caption on next page)

Fig. 3. SSBP1 interacts with p53 and facilitates p53 S15 phosphorylation to increase accumulation of nuclear p53 in high fructose-stimulated glomerular podocyte ferroptosis. (A) Lysates from high fructose-cultured podocytes were incubated with *anti*-SSBP1, and the co-eluted proteins were examined using p53 antibody (n = 3 per group). (B–E) Podocytes were transfected with *SSBP1* plasmid or siRNA and the respective negative control. The mRNA level of p53 was measured by qPCR (n = 6 per group). Western blot analysis of the protein level of total p53 protein in podocytes (n = 6 per group). (F–I) Western blot analysis of the protein level of total and nucleus p53 in high fructose-stimulated rat glomeruli and podocytes (n = 6 per group). (J) Immunofluorescence staining of SSBP1 and p53 in high fructose-cultured podocytes (scale bras: 20 μm) (n = 3 per group). (K–L) Western blot analysis of the protein level of p53 S15 phosphorylation in high fructose-exposed rat glomeruli and podocytes (n = 6 per group). (M) Podocytes were transfected with Myc-Wt p53 or Myc-Mut p53 and cultured with or without 5 mM fructose for 96 h. Podocytes were then used to isolate whole cell lysates (WCL), cytoplasmic (Cyto) and nuclear (Nucl) fractions, respectively. Aliquots relative to same cell number per component were immunoblotted using *anti*-Myc antibody (n = 3 per group). Lamin B1 and GAPDH were used as the control of nuclear and cytoplasmic fraction, respectively. (N–P) Podocytes were transfected with *SSBP1* siRNA as well as negative control and then cultured with or without fructose (5 mM). Western blot analysis of the protein level of p53 S15 phosphorylation and nucleus p53 in podocytes (n = 6 per group). Immunofluorescence staining of p53 in podocytes. (scale bras: 20 μm) (n = 3 per group). Data are plotted as mean ± SEM. *P*-values were acquired by one-way ANOVA, n.s., no significance, $^{*}P < 0.05$, $^{**}P < 0.01$, $^{***}P < 0.001$.

3.5. SSBP1 is inhibited by pterostilbene to suppress DNA-PK/p53 pathway in the alleviation of high fructose-induced glomerular podocyte ferroptosis

We next examined if anti-oxidative agent pterstilbene could alleviate podocyte ferroptosis. Pterstilbene obviously decreased protein levels of SSBP1, p-DNA-PKcs(S2056), p-p53(S15) and nucleus p53, as well as upregulated SLC7A11 and GPX4 protein levels in high fructose-stimulated rat glomeruli and cultured podocytes (Fig. 5A-B and Supplemental Fig. 5A-B). Pterstilbene also decreased SSBP1 mRNA levels in *in vivo* and *in vitro* models (Supplemental Fig. 5C-D). It downregulated DNA-PK activity in high fructose-exposed podocytes (Supplemental Fig. 5E). Consistently, pterstilbene increased GSH, and decreased lipid peroxidation and MDA in *in vivo* and *in vitro* models (Fig. 5C-E and Supplemental Fig. 5F-G). Subsequently, high fructose-induced cell death in rat glomeruli and cultured podocytes was alleviated by pterstilbene (Fig. 5F-G). As expected [40,41], glomerular injury including upregulation of the ratio of urinary albumin to creatinine and glomerular mesangial expansion was alleviated by pterostilbene (Supplemental Fig. 5H-J). We also found that pterostilbene improved high fructose-induced mitochondrial morphology disruption and dysfunction in podocytes (Supplemental Fig. 5K-N). Pioglitazone, a peroxisome proliferator-activated receptor gamma agonist, which is known to inhibit mitochondrial iron uptake, lipid peroxidation and subsequent ferroptosis in hepatocellular carcinoma cells [42], and prevent podocyte injury [43], was used as positive control in this study. Pioglitazone exerted the similar effects in *in vitro* and *in vivo* models (Fig. 5A-G and Supplemental Fig. 5A-N). These data indicated that pterstilbene may reduce SSBP1 and suppress DNA-PK/p53 pathway to alleviate high fructose-induced glomerular podocyte ferroptosis.

4. Discussion

Ferroptosis is distinct from other programmed cell death with its unique morphological and bioenergetics features [44]. High fructose increases hepatic glutathione disulfide and MDA levels with ferroptosis in mouse model of non-alcoholic fatty liver disease [45]. Here, our study revealed that high dietary fructose consumption induced glomerular podocyte ferroptosis (main features of low-expression of ferroptosis protein markers SLC7A11 and GPX4, lipid peroxidation accumulation and cell death), which could be reversed by ferroptosis inhibitors.

SSBP1 is essential for mtDNA replication, and its dysfunction may affect mtDNA content, resulting in mitochondrial morphological and functional changes [46]. A recent report describes that p.G40V mutation of SSBP1 shows significant upregulation of SSBP1 expression, thereby decreases mtDNA content and mitochondrial energetic function in fibroblasts [22]. SSBP1 expression is increased with partial loss of mtDNA and ultimately triggers stress response and mitophagy in LONP1-depleted fibroblasts [47]. Here, we demonstrated that SSBP1 expression was dominantly increased in high fructose-stimulated rat glomeruli and cultured podocytes, and further depleted content of mtDNA. Consistently, we found high fructose induced mitochondrial morphology disruption and dysfunction in glomerular podocyte injury.

Recently, deletion of SSBP1 in fibroblasts is reported to reduce p53 expression at protein level rather than at mRNA level. In contrast, SSBP1 overexpression reinforces p53 protein level and then reduces cell viability [24]. Our results provided a previously unrevealed molecular mechanism by which high fructose induced podocyte ferroptosis by the SSBP1-p53 interaction. As mentioned above, p53 positively regulates ferroptosis by binding to the promoter region of SLC7A11 in nutlin 3-stimulated osteosarcoma cells [12]. Thus, the promotion of p53 nuclear retention leads to cell-cycle arrest, apoptosis and ferroptosis in lung cancer cells [48]. Here, we found that nuclear import of p53 was increased in high fructose-treated rat glomeruli and cultured podocytes. Several studies show that enhanced nuclear translocation of p53 can be regulated by its phosphorylation at serine 392, 249 and 20 sites in lung or liver cancer cells, and porcine epidemic diarrhea virus-infected Vero cells [36,49,50]. In this study, we observed the increase of p53 S15 phosphorylation in high fructose-exposed rat glomeruli and cultured podocytes. We also found that p53 with S15 mutation was inhibited to translocate into the nuclei in podocytes transfected with Myc-Wt p53 or Myc-Mut p53, respectively, and incubated with high fructose. Moreover, depletion of SSBP1 in high fructose-cultured podocytes decreased p53 S15 phosphorylation and its further nuclear accumulation. These results demonstrated that SSBP1 specifically induced p53 phosphorylation at S15 to enhance p53 nuclear localization in high fructose-exposed glomerular podocyte ferroptosis.

Of note, DNA-PK phosphorylates p53 at S15 and enhances p53 transcriptional activity in genotoxic stress-activated retina cells [51]. Activation of the programmed cell death through DNA-PK is proposed because DNA-PK is recruited to the p21 promoter and forms a protein complex with p53 in doxorubicin and chromium-stimulated colon carcinoma cells [52]. However, the role of DNA-PK in high fructose-induced ferroptosis has not been fully investigated. In this study, we found that SSBP1 promoted DNA-PK activation by directly interacting with DNA-PKcs in cultured podocytes after high fructose stimulation. Furthermore, SSBP1 and DNA-PKcs formed a protein complex with p53 to increase its phosphorylation. Our results indicated that SSBP1 enhanced DNA-PK activity to induce p53 phosphorylation and thus accelerate podocyte ferroptosis in high fructose-stimulated glomerular injury.

Antioxidants, such as trolox, butylated hydroxyltoluence, Tiron and TEMPO, are reported to reduce erastin-induced ferroptosis in fibrosarcoma cells [53]. Pterostilbene is a natural dimethylated resveratrol analog found primarily in blueberries and *Pterocarpus marsupium* heartwood [26,40]. Pterostilbene is known for its anti-oxidation activity among several pharmacological properties [54]. It inhibits ROS-mediated mitochondrial apoptosis in hepatocellular carcinoma [25], and suppresses apoptosis in arsenic-induced human keratinocytes and streptozotocin-induced diabetic rats [55,56]. Our previous study showed that pterostilbene attenuated high fructose-induced kidney oxidative stress and fibrosis in rats [26,27]. Here, we found the inhibitory effect of anti-oxidant pterostilbene on high fructose-induced glomerular podocyte ferroptosis. Pterostilbene eliminated

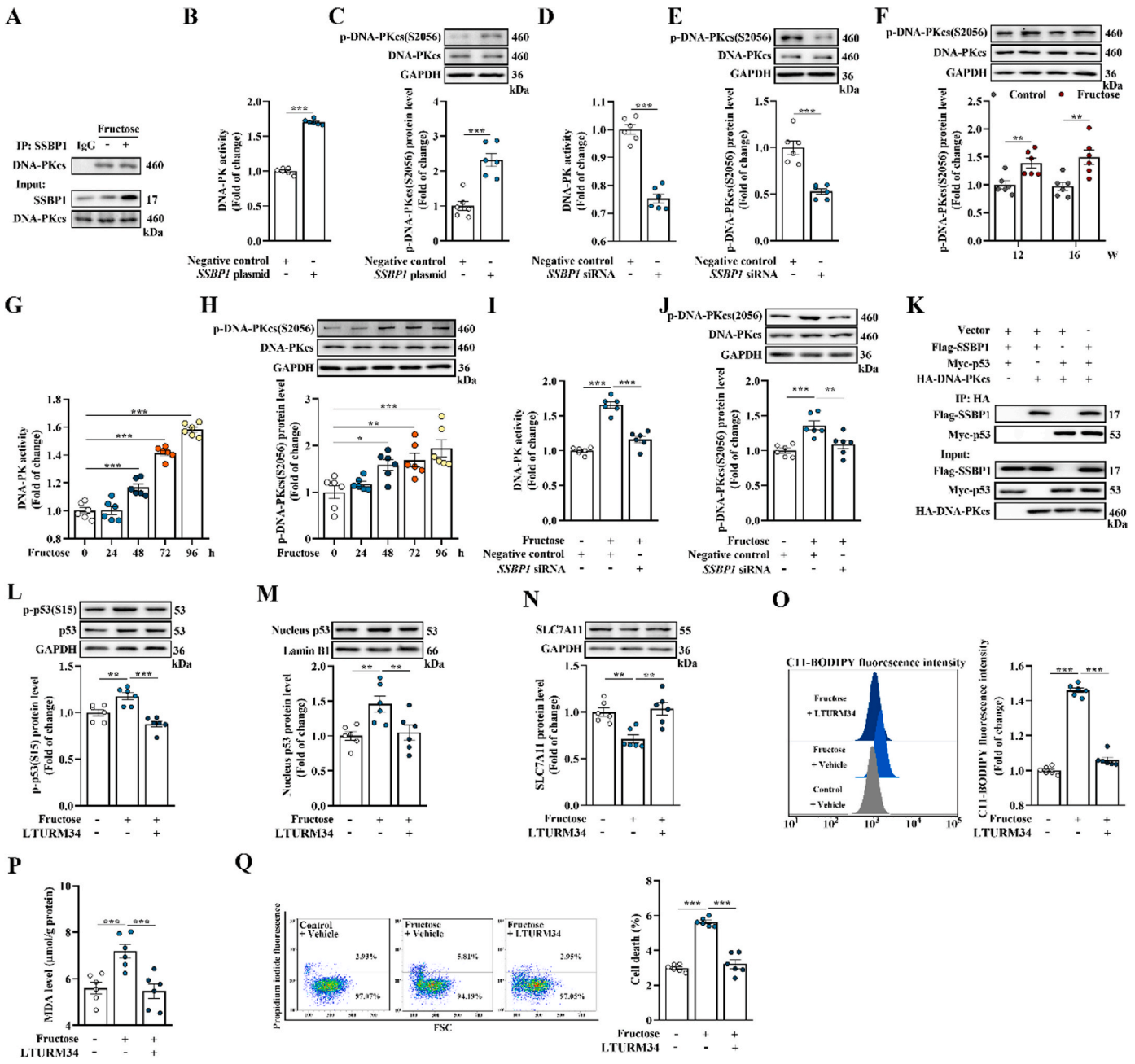

Fig. 4. SSBP1 activates DNA-PK to phosphorylate p53 in high fructose-induced glomerular podocytes ferroptosis. (A) Lysates from high fructose-cultured podocytes were incubated with *anti*-SSBP1, and the co-eluted proteins were examined using DNA-PKcs antibody (n = 3 per group). (B–C) Podocytes were transfected with *SSBP1* plasmid and negative control. DNA-PK activity in podocytes was measured by assay kit (n = 6 per group). Western blot analysis of the protein level of DNA-PKcs S2056 phosphorylation in podocytes (n = 6 per group). (D–E) Podocytes were transfected with *SSBP1* siRNA and negative control. DNA-PK activity in podocytes was measured by assay kit (n = 6 per group). Western blot analysis of the protein level of DNA-PKcs S2056 phosphorylation in podocytes (n = 6 per group). (F) Western blot analysis of the protein level of DNA-PKcs S2056 phosphorylation in high fructose-stimulated rat glomeruli (n = 6 per group). (G) DNA-PK activity in high fructose-cultured podocytes was measured by assay kit (n = 6 per group). (H) Western blot analysis of the protein level of DNA-PKcs S2056 phosphorylation in high fructose-cultured podocytes (n = 6 per group). (I–J) Podocytes transfected with *SSBP1* siRNA or negative control and then cultured with or without fructose (5 mM). DNA-PK activity was measured by assay kit in podocytes (n = 6 per group). Western blot analysis of the protein level of DNA-PKcs S2056 phosphorylation in podocytes (n = 6 per group). (K) Flag-SSBP1, Myc-p53 and HA-DNA-PKcs were expressed alone or in combination in podocytes and Co-IP assays were performed using *anti*-HA antibody (n = 3 per group). (L–Q) Podocytes were cultured with or without fructose (5 mM) in the presence or absence of vehicle or DNA-PK inhibitor LTURM34. Western blot analysis of the protein levels of p53 S15 phosphorylation, nucleus p53 and SLC7A11 in podocytes (n = 6 per group). Lipid peroxidation in podocytes was analyzed by C11-BODIPY (581/591) staining and measured by flow cytometer (n = 6 per group). The MDA level was measured by assay kit in podocytes (n = 6 per group). Podocyte death was analyzed by propidium iodide staining and measured by flow cytometer (n = 6 per group). Data are plotted as mean ± SEM. *P*-values were acquired by one-way ANOVA, $^{*}P < 0.05$, $^{**}P < 0.01$, $^{***}P < 0.001$.

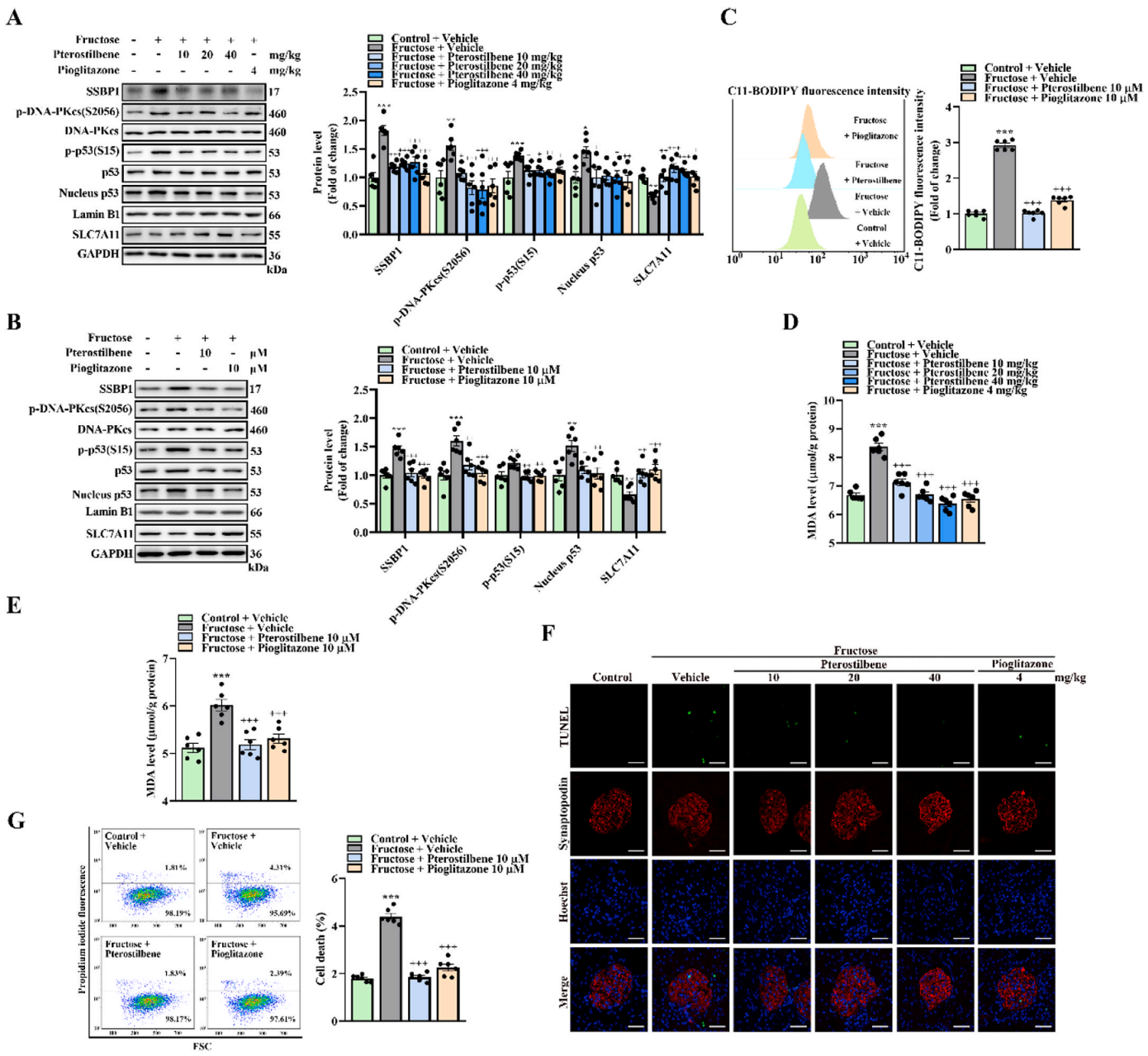

Fig. 5. SSBP1 is inhibited by pterostilbene to suppress DNA-PK/p53 pathway in the alleviation of high fructose-induced glomerular podocyte ferroptosis. (A) Rats were assigned into control group with a standard water and high fructose group fed with 10% fructose solution(W/V) for 16 weeks. After 8-week fructose intake, high fructose-fed rats were randomized into 5 subgroups, receiving water (vehicle), 10, 20 and 40 mg/kg pterostilbene, and 4 mg/kg pioglitazone for the next 8 weeks. Western blot analysis of the protein levels of SSBP1, p-DNA-PKcs(S2056), p-p53(S15), nucleus p53 and SLC7A11 in rat glomeruli (n = 6 per group). (B) Podocytes were cultured with or without fructose (5 mM), pterostilbene (10 μM) and pioglitazone (10 μM). Western blot analysis of the protein levels of SSBP1, p-DNA-PKcs (S2056), p-p53(S15), nucleus p53 and SLC7A11 in podocytes (n = 6 per group). (C) Lipid peroxidation in podocytes was analyzed by C11-BODIPY (581/591) staining and measured by flow cytometer (n = 6 per group). (D–E) The MDA level was measured by assay kit in rat glomeruli and podocytes (n = 6 per group). (F) Cell death was analyzed by TUNEL staining in rat glomeruli. Green fluorescence in pictures represented positive signals (cell death) (scale bras: 20 μm) (n = 3 per group). (G) Podocyte death was analyzed by propidium iodide staining and measured by flow cytometer (n = 6 per group). Data are plotted as mean ± SEM. *P*-values were acquired by one-way ANOVA, $^{*}P < 0.05$, $^{**}P < 0.01$, $^{***}P < 0.001$ *vs* control vehicle group, $^{+}P < 0.05$, $^{++}P < 0.01$, $^{+++}P < 0.001$ *vs* fructose vehicle group.

mitochondrial ROS and improved mitochondrial morphology disruption in high fructose-exposed glomerular podocytes. More importantly, pterostilbene decreased SSBP1 expression, inhibited DNA-PK/p53 pathway, upregulated SLC7A11 and GXP4 expression, subsequently alleviated lipid peroxidation accumulation and podocyte ferroptosis in high fructose-induced glomerular injury. These results further demonstrated that SSBP1 downregulation may suppress DNA-PK/p53 pathway to attenuate high fructose-caused glomerular podocyte ferroptosis.

Collectively, this study demonstrated that high fructose triggered podocyte ferroptosis in glomerular injury. Moreover, the enhanced SSBP1 induced podocyte ferroptosis via activating DNA-PK/p53 pathway in high fructose-induced glomerular injury. Hence, our study provides a novel targeting strategy for high fructose-induced ferroptotic cell death and suggests that inhibition of SSBP1 by pterostilbene may be a potential therapeutic approach in high fructose-induced podocyte ferroptosis.

Authors' contributions

Ling-Dong Kong conceived the study. Ling-Dong Kong and Lei Fang designed the study; Wen-Yuan Wu performed *in vivo* and *in vitro* experiments; Tu-Shuai Li, Xiao-Qin Ding, Zhi-Hong Liu and Jie Yang helped animal experiments; Wen-Yuan Wu and Zi-Xuan Wang analyzed the data; Ling-Dong Kong, Lei Fang, Wen-Yuan Wu and Zi-Xuan Wang wrote the manuscript.

Declaration of competing interest

The authors declare that there is no conflict of interest.

Acknowledgment

This work was supported by Grant from National Natural Science Foundation of China (Nos. 81730105 and 81991522), and partly from the Open Project of State Key Laboratory of Natural Medicines, No. SKLNMKF202204.

Appendix A. Supplementary data

Supplementary data to this article can be found online at https://doi.org/10.1016/j.redox.2022.102303.

References

[1] M. Nagata, Podocyte injury and its consequences, Kidney Int. 89 (6) (2016) 1221–1230, https://doi.org/10.1016/j.kint.2016.01.012.
[2] E. Torban, F. Braun, N. Wanner, T. Takano, P.R. Goodyer, R. Lennon, P, et al., From podocyte biology to novel cures for glomerular disease, Kidney Int. 96 (4) (2019) 850–861, https://doi.org/10.1016/j.kint.2019.05.015.
[3] T.S. Li, L. Chen, S.C. Wang, Y.Z. Yang, H.J. Xu, H.M. Gu, et al., Magnesium isoglycyrrhizinate ameliorates fructose-induced podocyte apoptosis through downregulation of miR-193a to increase WT1, Biochem. Pharmacol. 166 (2019) 139–152, https://doi.org/10.1016/j.bcp.2019.05.016.
[4] P.D. Prince, C.R. Lanzi, J.E. Toblli, R. Elesgaray, P.I. Oteiza, C.G. Fraga, et al., Dietary (-)-epicatechin mitigates oxidative stress, NO metabolism alterations, and inflammation in renal cortex from fructose-fed rats, Free Radic. Biol. Med. 90 (2016) 35–46, https://doi.org/10.1016/j.freeradbiomed.2015.11.009.
[5] J. Li, F. Cao, H.L. Yin, Z.J. Huang, Z.T. Lin, N. Mao, et al., Ferroptosis: past, present and future, Cell Death Dis. 11 (2) (2020) 88, https://doi.org/10.1038/s41419-020-2298-2.
[6] Y. Xie, W. Hou, X. Song, Y. Yu, J. Huang, X. Sun, et al., Ferroptosis: process and function, Cell Death Differ. 23 (3) (2016) 369–379, https://doi.org/10.1038/cdd.2015.158.
[7] P. Koppula, L. Zhuang, B. Gan, Cystine transporter SLC7A11/xCT in cancer: ferroptosis, nutrient dependency, and cancer therapy, Protein Cell 12 (8) (2021) 599–620, https://doi.org/10.1007/s13238-020-00789-5.
[8] J. Liu, X. Xia, P. Huang, xCT: a critical molecule that links cancer metabolism to redox signaling, Mol. Ther. 28 (11) (2020) 2358–2366, https://doi.org/10.1016/j.ymthe.2020.08.021.
[9] F. Ursini, M. Maiorino, Lipid peroxidation and ferroptosis: the role of GSH and GPx4, Free Radic. Biol. Med. 152 (2020) 175–185, https://doi.org/10.1016/j.freeradbiomed.2020.02.027.
[10] M.J. Duffy, N.C. Synnott, S. O'Grady, J. Crown, Targeting p53 for the treatment of cancer, Semin. Cancer Biol. (2020), https://doi.org/10.1016/j.semcancer.2020.07.005.
[11] Y. Wang, L. Yang, X. Zhang, W. Cui, Y. Liu, Q.R. Sun, et al., Epigenetic regulation of ferroptosis by H2B monoubiquitination and p53, EMBO Rep. 20 (7) (2019), e47563, https://doi.org/10.15252/embr.201847563.
[12] L. Jiang, N. Kon, T. Li, S.J. Wang, T. Su, H. Hibshoosh, et al., Ferroptosis as a p53-mediated activity during tumour suppression, Nature 520 (7545) (2015) 57–62, https://doi.org/10.1038/nature14344.
[13] D. Thomasova, H.A. Bruns, V. Kretschmer, M. Ebrahim, S. Romoli, H. Liapis, et al., Murine double minute-2 prevents p53-overactivation-related cell death (podoptosis) of podocytes, J. Am. Soc. Nephrol. 26 (7) (2015) 1513–1523, https://doi.org/10.1681/ASN.2014040345.
[14] M. Medova, M. Medo, L. Hovhannisyan, C. Munoz-Maldonado, D.M. Aebersold, Y. Zimmer, DNA-PK in human malignant disorders: mechanisms and implications for pharmacological interventions, Pharmacol. Ther. 215 (2020) 107617, https://doi.org/10.1016/j.pharmthera.2020.107617.
[15] H. Zhou, W. Du, Y. Li, C. Shi, N. Hu, S. Ma, et al., Effects of melatonin on fatty liver disease: the role of NR4A1/DNA-PKcs/p53 pathway, mitochondrial fission, and mitophagy, J. Pineal Res. 64 (1) (2018), https://doi.org/10.1111/jpi.12450.
[16] L. Song, T.Y. Chen, X.J. Zhao, Q. Xu, R.Q. Jiao, J.M. Li, et al., Pterostilbene prevents hepatocyte epithelial-mesenchymal transition in fructose-induced liver fibrosis through suppressing miR-34a/Sirt1/p53 and TGF-beta1/Smads signalling, Br. J. Pharmacol. 176 (11) (2019) 1619–1634, https://doi.org/10.1111/bph.14573.
[17] V. Diaz-Aguirre, C. Velez-Pardo, M. Jimenez-Del-Rio, Fructose sensitizes Jurkat cells oxidative stress-induced apoptosis via caspase-dependent and caspase-independent mechanisms, Cell Biol. Int. 40 (11) (2016) 1162–1173, https://doi.org/10.1002/cbin.10653.
[18] L. Fang, T.S. Li, J.Z. Zhang, Z.H. Liu, J. Yang, B.H. Wang, et al., Fructose drives mitochondrial metabolic reprogramming in podocytes via Hmgcs2-stimulated fatty acid degradation, Signal Transduct. Target. Ther. 6 (1) (2021) 253, https://doi.org/10.1038/s41392-021-00570-y.
[19] M.J. Young, W.C. Copeland, Human mitochondrial DNA replication machinery and disease, Curr. Opin. Genet. Dev. 38 (2016) 52–62, https://doi.org/10.1016/j.gde.2016.03.005.
[20] F. Zhang, Z. Dong, S. Gao, G. Chen, D. Liu, AT1R-mediated apoptosis of bone marrow mesenchymal stem cells is associated with mtROS production and mtDNA reduction, 2019, Oxid. Med. Cell. Longev. (2019), 4608165, https://doi.org/10.1155/2019/4608165.
[21] X. Wang, X. Li, S. Liu, A.N. Brickell, J. Zhang, Z. Wu, et al., PCSK9 regulates pyroptosis via mtDNA damage in chronic myocardial ischemia, Basic Res. Cardiol. 115 (6) (2020) 66, https://doi.org/10.1007/s00395-020-00832-w.
[22] V. Del Dotto, F. Ullah, I. Di Meo, P. Magini, M. Gusic, A. Maresca, et al., SSBP1 mutations cause mtDNA depletion underlying a complex optic atrophy disorder, J. Clin. Invest. 130 (1) (2020) 108–125, https://doi.org/10.1172/JCI128514.
[23] M.A. Gustafson, E.M. McCormick, L. Perera, M.J. Longley, R. Bai, J. Kong, et al., Mitochondrial single-stranded DNA binding protein novel de novo SSBP1 mutation in a child with single large-scale mtDNA deletion (SLSMD) clinically manifesting as Pearson, Kearns-Sayre, and Leigh syndromes, PLoS One 14 (9) (2019), e0221829, https://doi.org/10.1371/journal.pone.0221829.
[24] H.P. Tian, Y.H. Sun, L. He, Y.F. Yi, X. Gao, D.L. Xu, Single-stranded DNA-binding protein 1 abrogates cardiac fibroblast proliferation and collagen expression induced by angiotensin II, Int. Heart J. 59 (6) (2018) 1398–1408, https://doi.org/10.1536/ihj.17-650.
[25] L. Guo, K. Tan, H. Wang, X. Zhang, Pterostilbene inhibits hepatocellular carcinoma through p53/SOD2/ROS-mediated mitochondrial apoptosis, Oncol. Rep. 36 (6) (2016) 3233–3240, https://doi.org/10.3892/or.2016.5151.
[26] W. Wang, X.Q. Ding, T.T. Gu, L. Song, J.M. Li, Q.C. Xue, et al., Pterostilbene and allopurinol reduce fructose-induced podocyte oxidative stress and inflammation via microRNA-377, Free Radic. Biol. Med. 83 (2015) 214–226, https://doi.org/10.1016/j.freeradbiomed.2015.02.029.
[27] T.T. Gu, T.Y. Chen, Y.Z. Yang, X.J. Zhao, Y. Sun, T.S. Li, et al., Pterostilbene alleviates fructose-induced renal fibrosis by suppressing TGF-beta1/TGF-beta type I receptor/Smads signaling in proximal tubular epithelial cells, Eur. J. Pharmacol. 842 (2019) 70–78, https://doi.org/10.1016/j.ejphar.2018.10.008.
[28] G.M. Ducasa, A. Mitrofanova, S.K. Mallela, X. Liu, J. Molina, A. Sloan, et al., ATP-binding cassette A1 deficiency causes cardiolipin-driven mitochondrial dysfunction in podocytes, J. Clin. Invest. 129 (8) (2019) 3387–3400, https://doi.org/10.1172/JCI125316.
[29] Y.M. Feng, Y.F. Jia, L.Y. Su, D. Wang, L. Lv, L. Xu, et al., Decreased mitochondrial DNA copy number in the hippocampus and peripheral blood during opiate addiction is mediated by autophagy and can be salvaged by melatonin, Autophagy 9 (9) (2013) 1395–1406, https://doi.org/10.4161/auto.25468.
[30] S. Neitemeier, A. Jelinek, V. Laino, L. Hoffmann, I. Eisenbach, R. Eying, et al., BID links ferroptosis to mitochondrial cell death pathways, Redox Biol. 12 (2017) 558–570, https://doi.org/10.1016/j.redox.2017.03.007.
[31] L. Chen, J. Yang, S.J. Zhao, T.S. Li, R.Q. Jiao, L.D. Kong, Atractylodis rhizoma water extract attenuates fructose-induced glomerular injury in rats through anti-oxidation to inhibit TRPC6/p-CaMK4 signaling, Phytomedicine 91 (2021) 153643, https://doi.org/10.1016/j.phymed.2021.153643.
[32] C. Oudot, A.D. Lajoix, B. Jover, C. Rugale, Dietary sodium restriction prevents kidney damage in high fructose-fed rats, Kidney Int. 83 (4) (2013) 674–683, https://doi.org/10.1038/ki.2012.478.
[33] H.N. Choi, Y.H. Park, J.H. Kim, M.J. Kang, S.M. Jeong, H.H. Kim, et al., Renoprotective and antioxidant effects of Saururus chinensis Baill in rats fed a high-fructose diet, Nutr. Res. Pract. 5 (4) (2011) 365–369, https://doi.org/10.4162/nrp.2011.5.4.365.
[34] M. Falkenberg, Mitochondrial DNA replication in mammalian cells: overview of the pathway, Essays Biochem. 62 (3) (2018) 287–296, https://doi.org/10.1042/EBC20170100.
[35] C. Piro-Megy, E. Sarzi, A. Tarres-Sole, M. Pequignot, F. Hensen, M. Quiles, et al., Dominant mutations in mtDNA maintenance gene SSBP1 cause optic atrophy and foveopathy, J. Clin. Invest. 130 (1) (2020) 143–156, https://doi.org/10.1172/JCI128513.
[36] S. Song, Y. Shi, W. Wu, H. Wu, L. Chang, P. Peng, et al., Reticulon 3-mediated Chk2/p53 activation suppresses hepatocellular carcinogenesis and is blocked by hepatitis B virus, Gut (2020), https://doi.org/10.1136/gutjnl-2020-321386.
[37] S.H. Jung, H.J. Hwang, D. Kang, H.A. Park, H.C. Lee, D. Jeong, et al., mTOR kinase leads to PTEN-loss-induced cellular senescence by phosphorylating p53, Oncogene 38 (10) (2019) 1639–1650, https://doi.org/10.1038/s41388-018-0521-8.
[38] E.R. Wolf, C.P. McAtarsney, K.E. Bredhold, A.M. Kline, L.D. Mayo, Mutant and wild-type p53 form complexes with p73 upon phosphorylation by the kinase JNK, Sci. Signal. 11 (524) (2018), https://doi.org/10.1126/scisignal.aao4170.
[39] D. Ma, X. Chen, P.Y. Zhang, H. Zhang, L.J. Wei, S. Hu, et al., Upregulation of the ALDOA/DNA-PK/p53 pathway by dietary restriction suppresses tumor growth, Oncogene 37 (8) (2018) 1041–1048, https://doi.org/10.1038/onc.2017.398.
[40] Y.J. Wang, Y.Y. Chen, C.M. Hsiao, M.H. Pan, B.J. Wang, Y.C. Chen, et al., Induction of autophagy by pterostilbene contributes to the prevention of renal fibrosis via

attenuating NLRP3 inflammasome activation and epithelial-mesenchymal transition, Front. Cell Dev. Biol. 8 (2020) 436, https://doi.org/10.3389/fcell.2020.00436.
[41] J. Pan, M. Shi, L.Z. Li, J. Liu, F. Guo, Y.H. Feng, et al., Pterostilbene, a bioactive component of blueberries, alleviates renal fibrosis in a severe mouse model of hyperuricemic nephropathy, Biomed. Pharmacother. 109 (2019) 1802–1808, https://doi.org/10.1016/j.biopha.2018.11.022.
[42] H. Yuan, X. Li, X. Zhang, R. Kang, D. Tang, CISD1 inhibits ferroptosis by protection against mitochondrial lipid peroxidation, Biochem. Biophys. Res. Commun. 478 (2) (2016) 838–844, https://doi.org/10.1016/j.bbrc.2016.08.034.
[43] T. Kanjanabuch, L.J. Ma, J. Chen, A. Pozzi, Y. Guan, P. Mundel, et al., PPAR-gamma agonist protects podocytes from injury, Kidney Int. 71 (12) (2007) 1232–1239, https://doi.org/10.1038/sj.ki.5002248.
[44] Z. Zhang, M. Guo, M. Shen, D. Kong, F. Zhang, J. Shao, et al., The BRD7-P53-SLC25A28 axis regulates ferroptosis in hepatic stellate cells, Redox Biol. 36 (2020) 101619, https://doi.org/10.1016/j.redox.2020.101619.
[45] J.H. Pan, H. Cha, J. Tang, S. Lee, S.H. Lee, B. Le, et al., The role of microRNA-33 as a key regulator in hepatic lipogenesis signaling and a potential serological biomarker for NAFLD with excessive dietary fructose consumption in C57BL/6N mice, Food Funct. 12 (2) (2021) 656–667, https://doi.org/10.1039/d0fo02286a.
[46] N. Jurkute, C. Leu, H.M. Pogoda, G. Arno, A.G. Robson, G. Nurnberg, et al., SSBP1 mutations in dominant optic atrophy with variable retinal degeneration, Ann. Neurol. 86 (3) (2019) 368–383, https://doi.org/10.1002/ana.25550.
[47] O. Zurita Rendon, E.A. Shoubridge, LONP1 is required for maturation of a subset of mitochondrial proteins, and its loss elicits an integrated stress response, Mol. Cell Biol. 38 (20) (2018), https://doi.org/10.1128/MCB.00412-17.
[48] C. Mao, X. Wang, Y. Liu, M. Wang, B. Yan, Y. Jiang, et al., A G3BP1-interacting lncRNA promotes ferroptosis and apoptosis in cancer via nuclear sequestration of p53, Cancer Res. 78 (13) (2018) 3484–3496, https://doi.org/10.1158/0008-5472.CAN-17-3454.
[49] P. Liao, S.X. Zeng, X. Zhou, T. Chen, F. Zhou, B. Cao, et al., Mutant p53 gains its function via c-Myc activation upon CDK4 phosphorylation at serine 249 and consequent PIN1 binding, Mol. Cell. 68 (6) (2017) 1134–1146, https://doi.org/10.1016/j.molcel.2017.11.006.
[50] X. Xu, Y. Xu, Q. Zhang, F. Yang, Z. Yin, L. Wang, et al., Porcine epidemic diarrhea virus infections induce apoptosis in Vero cells via a reactive oxygen species (ROS)/p53, but not p38 MAPK and SAPK/JNK signalling pathways, Vet. Microbiol. 232 (2019) 1–12, https://doi.org/10.1016/j.vetmic.2019.03.028.
[51] T.Y. Chen, B.M. Huang, T.K. Tang, Y.Y. Chao, X.Y. Xiao, P.R. Lee, et al., Genotoxic stress-activated DNA-PK-p53 cascade and autophagy cooperatively induce ciliogenesis to maintain the DNA damage response, Cell Death Differ. 28 (6) (2021) 1865–1879, https://doi.org/10.1038/s41418-020-00713-8.
[52] R. Hill, P.A. Madureira, D.M. Waisman, P.W. Lee, DNA-PKCS binding to p53 on the p21WAF1/CIP1 promoter blocks transcription resulting in cell death, Oncotarget 2 (12) (2011) 1094–1108, https://doi.org/10.18632/oncotarget.378.
[53] S.J. Dixon, K.M. Lemberg, M.R. Lamprecht, R. Skouta, E.M. Zaitsev, C.E. Gleason, et al., Ferroptosis: an iron-dependent form of nonapoptotic cell death, Cell 149 (5) (2012) 1060–1072, https://doi.org/10.1016/j.cell.2012.03.042.
[54] S.A. Malik, J.D. Acharya, N.K. Mehendale, S.S. Kamat, S.S. Ghaskadbi, Pterostilbene reverses palmitic acid mediated insulin resistance in HepG2 cells by reducing oxidative stress and triglyceride accumulation, Free Radic. Res. 53 (7) (2019) 815–827, https://doi.org/10.1080/10715762.2019.1635252.
[55] J. Zhou, X. Ci, X. Ma, Q. Yu, Y. Cui, Y. Zhen, et al., Pterostilbene activates the Nrf2-dependent antioxidant response to ameliorate arsenic-induced intracellular damage and apoptosis in human keratinocytes, Front. Pharmacol. 10 (2019) 497, https://doi.org/10.3389/fphar.2019.00497.
[56] S. Ozdas, B. Tastekin, S.G. Gurgen, T. Ozdas, A. Pelit, S.O. Erkan, et al., Pterostilbene protects cochlea from ototoxicity in streptozotocin-induced diabetic rats by inhibiting apoptosis, PLoS One 15 (7) (2020), e0228429, https://doi.org/10.1371/journal.pone.0228429.